Modeling Coupled Migration and Settling of Particulates in Curing Filled Epoxies

Lisa Mondy, Rekha Rao, Eric Lindgren, Amy Sun, Doug Adolf, Charles Retallack, Kyle Thompson

Sandia National Laboratories, Albuquerque, New Mexico 87185

Received 14 December 2010; accepted 9 May 2010
DOI 10.1002/app.34425
Published online 31 May 2011 in Wiley Online Library (wileyonlinelibrary.com).

ABSTRACT: Epoxy resins filled to a high solids loading (40–60% by volume) with noncolloidal particles are used to mitigate stress and vibration in electronic components. We perform continuum-level finite element method (Schunk et al., A Full-Newton Finite Element Program for Free and Moving Boundary Problems with Coupled Fluid/Solid Momentum, Energy, Mass, and Chemical Species Transport: User's Guide, Sandia National Laboratories) simulations of filler particle redistribution during the nonisothermal cure of the epoxy under both quiescent and bulk flow conditions. An extent of reaction is used to track the degree of cure. To determine the particle migration, we couple a diffusive flux suspension model (Zhang and Acrivos, Int J Multiphase Flow 1994, 20, 579.) with the curing model. The heat transfer, including the exothermic polymerization reaction, is also modeled. The result is a generalized Newtonian model that has viscosity as a function of temperature, cure and particle volume fraction. With x-ray computed tomography, we examine settling of the particulate phase in both flowing and quiescent curing systems and compare the experimental results to the model predictions. The model is also validated with temperature measurements. © 2011 Wiley Periodicals, Inc. J Appl Polym Sci 122: 1587–1598, 2011

Key words: simulation; polymerization; sedimentation

INTRODUCTION

Filled polymers are found in manufacturing applications ranging from encapsulation of microelectronics to injection molding of composite parts. We specifically address epoxy composites, which are used to prevent corona discharges or catastrophic electrical arcs in high voltage electrical devices.[1] Similar filled epoxies are found in liquid molding technologies for the aerospace industry[2] and emerging technologies to develop functionally graded materials.[3] Developing predictive models of these manufacturing processes requires knowledge of time- and temperature-dependent rheology of the polymer.[2,4,5] The rheology of filled polymers is not only highly dependent on the extent of reaction of the polymerization or cure, but also on the particle volume fraction.[6,7] Furthermore, the local particle volume fraction can change due to gravity, convection, and shear-induced migration.[8–10] Even under quiescent conditions, gravity-driven particle settling in simple geometries with sharp features leads to instabilities and chaotic flow.[8] Shear induced migration during the mold fill and gravity-driven instabilities during the quiescent curing stage can lead to detrimental inhomogeneities in the final filler particle density. Although others have modeled simultaneous settling and curing,[7,11,12] these models are generally one-dimensional and do not take into account convective or shear-induced migration of particles. In this article, we couple continuum-level finite element method (FEM) simulations of filler particle redistribution during the nonisothermal cure of the epoxy under both bulk flow and quiescent conditions.

Systems of interest are epoxy resins filled with a high loading (40–60% by volume) of solid noncolloidal particles. Particle volume fraction gradients in such suspensions have been shown to develop in flows in which a shear gradient occurs, as particles are driven away from the high-shear-rate regions.[9] This particle migration occurs even in creeping flow and in the absence of significant nonhydrodynamic effects. Phillips et al.[13] distilled Leighton and Acrivos's [9] scaling arguments to develop a set of continuum constitutive equations based on three major causes of particle migration, which are gradients in shear-rate, particle volume fraction and relative viscosity. The Phillips model, also called the diffusive-flux model, uses a particle- volume fraction-

Correspondence to: L. Mondy (lamondy@sandia.gov).
Contract grant sponsor: United States Department of Energy; contract grant number: DEAC04-94AL85000.
Contract grant sponsor: U.S. Department of Energy, Office of Science, Advanced Scientific Computing Research Program.

dependent generalized Newtonian viscosity coupled with a diffusion equation to track the evolution of the particle volume fraction.

The formation of steep, gravity-induced, particle volume fraction gradients with distinct clearing regions can occur in filled epoxies but is often undesirable. Zhang and Acrivos[14] extended a diffusive-flux model to account for effects caused by non-neutrally buoyant particles in suspension. Rao et al.[8,10] used a similar model to predict the settling of suspensions in a variety of geometries. Their computer predictions compared well to flow visualization data obtained with nuclear magnetic resonance imaging. Although other constitutive models have been postulated for viscous flows of neutrally buoyant suspensions,[16–18] this success in capturing the bulk of the phenomena described by more sophisticated models and the ease of implementation of this Phillips-type model in a generalized three-dimensional computer code have led us to choose the model of Rao et al., extending it to describe suspension flows in which polymerization of the epoxy resin is occurring.

Coupling suspension rheology with the thermal effect, driven by exothermic polymerization and the temperature program of the oven during the cure, is required to accurately simulate the viscosity as it evolves in time, an important parameter for particle redistribution. Here we present initial work in developing and validating a model that couples suspension behavior with epoxy kinetics. We use a general purpose computer code developed at Sandia, GOMA,[19] for continuum-level FEM simulations of filler particle redistribution during the nonisothermal cure of the epoxy under both bulk flow and quiescent conditions.

Lagasse and Thompson[20] have studied spatial gradients in particle volume fraction formed by gravitational sedimentation of immersed particles in reinforced polymers using two experimental techniques, x-ray attenuation and laser confocal microscopy. Here, we focus on x-ray attenuation and x-ray computed tomography (CT) to obtain model validation data in more complex geometries for glass-microballoon-filled epoxy systems similar to those studied by Lagasse and Thompson. Three geometries under quiescent and bulk flow conditions are considered. Two mold geometries are studied in which the bulk suspension is quiescent, although gravity drives convective flow. The simplest, a straight cylinder, is used to compare x-ray CT data with the earlier microscopy data by Lagasse and Thompson to help determine the potential of this x-ray technique for low density-contrast materials such as the microballoons-epoxy system. The results in a more complex mold geometry, in which gravity-induced instabilities can occur in otherwise quiescent settling of suspensions, are also presented. Finally, in the third geometry, flow of suspensions between counter-rotating concentric cylinders (a wide-gap Couette apparatus) is studied to provide cases in which flow-induced migration might occur to a larger extent.

In the next section, we describe the materials, define the three geometries that are studied, and explain the experimental techniques and measurements. The following section outlines the continuum suspension model, the effects of the extent of cure on the epoxy viscosity, the kinetics model for the cure, and the balance equations solved with GOMA. The Results section includes the details of the particular computer simulations performed and the comparison of the computational results with the experimental results. A summary and discussion of the work is presented in the final section.

EXPERIMENTS

Materials and property measurements

The epoxy we model is designated "459" and consists of Shell Epon® 826 (Shell Oil Products) cured with a mixture of Jeffamine® D-230 (Huntsman) and Ancamine® 2049 (Air Products and Chemicals). A second epoxy, Shell Epon 828 cured with diethanolamine (DEA, Huntsman), is used only in experiments to compare two techniques to determine particle volume fraction.

Both epoxies are filled with spherical, hollow, glass-microballoons (GMB, $3M^{TM}$ material D32/4500). The typical density of a single particle is 0.34 g/cm^3. The particles have a distribution of sizes, where the median of the volume distribution, corresponds to $D_{50} = 41$ μm. Likewise, D_{10} and D_{90} are 24 μm and 62 μm, respectively. The average volume fraction ϕ of the particles in suspension is 0.56.

The apparent viscosity of the liquid epoxy is a strong function of time through the extent of cure, the volume fraction of filler, and temperature. We relate the changing viscosity of curing thermosets to extent of reaction through a series of measurements during the time of cure.[4,5,21,22] Details of the formalism can be found in these references, but are briefly summarized here and in the Theory section.

First, isothermal experiments in a TA Instruments Q200 Differential Scanning Calorimeter (DSC) measure the heat produced with time. From these measurements, we determine the rate of reaction and the heat of reaction (for epoxy cure). A finite difference method is then used to determine the extent of reaction by integrating the reaction rate. The experimental values for the reaction rate and the extent of reaction are used to populate a kinetic model for

TABLE I
Oven Cycle

Initial T (°C)	Final T (°C)	Elapsed time (h)
54	23	0.3
23	23	2.5
23	93	3.0
93	93	2.0
93	23	1.0

condensation chemistry, a common approach for epoxy systems.

Viscosity measurements are carried out using a Rheometrics viscometer equipped with a Couette geometry. We measure the viscosities with time, at a steady shear rate and at the same temperatures as tested with the DSC, of the suspending fluid, and then these data are plotted against the extent of reaction. The equations relating the extent of reaction to the viscosity of the epoxy as it cures are discussed in the Theory section. There, we also detail the values of the equation parameters that best fit the measured data.

The viscosities of several suspensions of GMB in either the epoxy resin or the curative alone are also measured to determine the increase in the suspension viscosity with increasing GMB volume fraction independent from the effects of curing. Although some shear thinning of the suspensions is observed, we ignore that effect here. Viscosity data are compared to our model equations in the Theory section.

Geometries

The epoxy suspensions are cured in three geometries to provide validation data for the model described in the next section. In the first experiments, the epoxy suspension is cured in simple cylinders, in which the suspension is allowed to float during a programmed oven cure (Table I). The suspensions are separately prepared, degassed, preheated to 54°C, and poured into cylinders. The samples are then allowed to cure under quiescent conditions. These experiments are designed specifically to determine the flotation of the particles in the simplest geometry possible. Figure 1 shows the geometry of the sample of 828/DEA with suspended GMB. This sample was tested and reported by Lagasse and Thompson[20] and provides independent data with which to confirm the accuracy of the new CT radiography analysis. The 459 GMB cylinder is similar but taller. We cut two rectangular samples from the GMB molded material, each $\sim$ 10 mm long in the direction of gravity, with a 5-mm square cross section. The samples are taken along the axis of the mold, at the top and bottom of the mold, as also shown in Figure 1.

In the second experiment, the suspension of GMB in 459 is prepared and poured into an axisymmetric, strain-test Kovar™ mold, then cured using the same programmed oven schedule shown in Table I and under quiescent conditions. This mold geometry is shown in Figure 2. Here, the epoxy mix is poured around a closed Kovar tube, such that it fills the gap between the tube and the concentric outer mold. This test was designed primarily to measure solid properties once the cure had completed (the results of which are outside the scope of this paper). However, we were able to analyze the sample for particle volume fraction, as well as obtain the thermal data generated to validate our model. This geometry, with the inner suspended shape, has the potential to create density-driven instabilities as the particles are trapped on an interior horizontal surface (the underside of the end of the tube).[8]

Finally, we also tested the 459 GMB epoxy suspension under flow conditions. Here, we place the suspension between parallel concentric cylinders (a wide-gap Couette) and rotated the inner cylinder until vitrification. The axes of the cylinders were horizontal, perpendicular to the direction of gravity. Figure 3 shows the geometry of the apparatus. This geometry results in strong gradients in shear rate and has been shown to cause particle migration in ideal suspensions.[13] The Couette is also instrumented with thermocouples to measure the temperatures of the oven and epoxy during a cure.

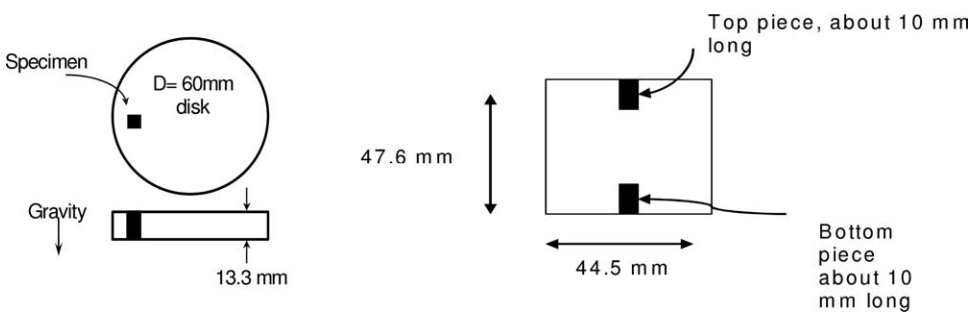

Figure 1 Sketch of simple disc geometries for 828/DEA (left) and 459 (right) filled with GMB.

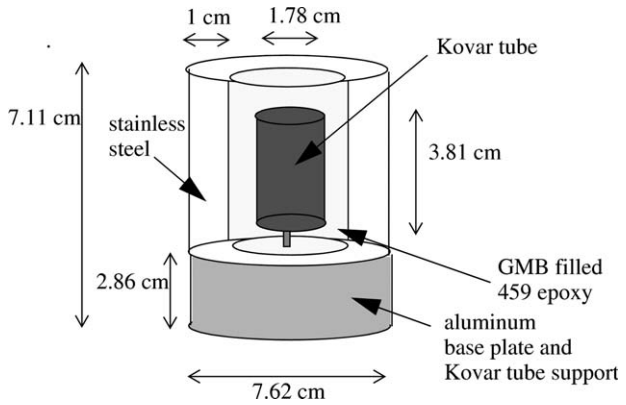

Figure 2 Sketch of Kovar tube mold.

X-ray imaging

Confocal microscopy, as described by Lagasse and Thompson,[20] requires the addition of a fluorescent dye. With this technique the particle volume fraction is determined by essentially counting each particle in a sample. Care must be taken that the sample is small enough to allow good resolution but large enough to be a representative sample of the volume fraction. Despite considerable operator judgment required during the image processing of the data, the experimental results can be reliably reproduced. Repeatability is demonstrated in Figure 4, which overlays the original Lagasse and Thompson data with a second set taken on the same sample (Fig. 1, left) but by a different operator[23] on a different microscope and analyzed by the authors without influence of the original results. Although the confocal microscopy results are impressive, a technique that could be faster, less operator intensive, and used without the addition of dye was sought.

Although conventional x-ray attenuation methods, such as used by Lagasse and Thompson[20] could not distinguish small changes in density between the epoxy and the hollow glass particles, x-ray CT was thought to be a candidate for this application. CT is a noncontact nondestructive inspection method that generates cross-sectional views (images) of the part being examined. When many of these images are combined, they form a three-dimensional representation of the part. These images are generated by measuring the x-ray attenuation through the part from various directions and then processing these data to produce a digital image (Fig. 5). The resulting three-dimensional image has intensity that is proportional to the material density. The proportionality constant is determined from images of materials of known density or from regions within the sample where the density is known.

A HYTEC FCT P-101 CT system coupled with a Kevex PXS10-65 microfocus x-ray machine is used to image the 459 GMB samples. This CT system has variable spatial resolution (dependent upon part size and system parameters). The image resolution of the parts varied from 9 μm, on the smaller samples, to 35 μm on the larger samples. X-ray energies ranging from 110 to 130 kV were used.

The x-ray CT technique also has drawbacks; in particular, the presence of any high-density material will severely reduce the contrast in the encapsulant, and the volume fraction of GMB will not be detectable. However, much larger samples can be tested; therefore, not only is the sample preparation easier, it is also easier to know the location of any point within the sample because multiple precision cuts are not required.

The results of x-ray CT tests of the 828/DEA GMB-filled sample described in Figure 1 are included in Figure 4. The central region of constant, nominal GMB density, known from the microscopy, is used as a calibration. The x-ray technique is susceptible to end effects, although this sample shows little because it is potted in clear epoxy (for the microscopy) and, therefore, does not have an edge with a high density gradient present. The x-ray data appear a bit more "smoothed" and miss the slight dip in volume fraction at about 2.5 mm from the bottom. However, those features in the confocal image may be in part due to the small sample depth in the microscope. Each point from the confocal microscope represents a sample near the surface roughly 400 μm along a side. The configuration of particles changes with depth from the surface and may not reflect the volume fraction averaged over a larger depth as done with the CT.

More significant, however, is that the x-ray CT misses the zone devoid of particles at the bottom of the sample. Clearly, here confocal microscopy has the advantage of higher resolution. The particle-free zone is less than 200-μm high, which in this case is far beyond the resolution of the finite element model. The height of the clear zone measured with the confocal microscope varies with the depth from the surface, ranging from 100 to 200 μm, again

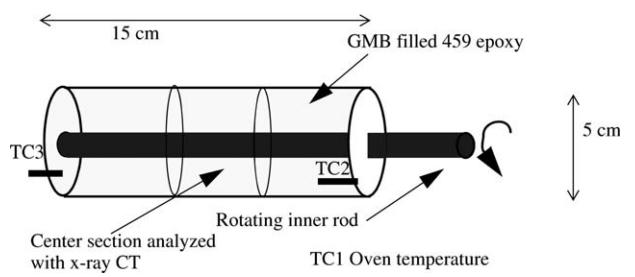

Figure 3 Geometry of Couette apparatus. The thermocouple locations are designated by "TC." TC2 is 2.5 cm into the epoxy from the front wall, and TC3 is just inside the back wall.

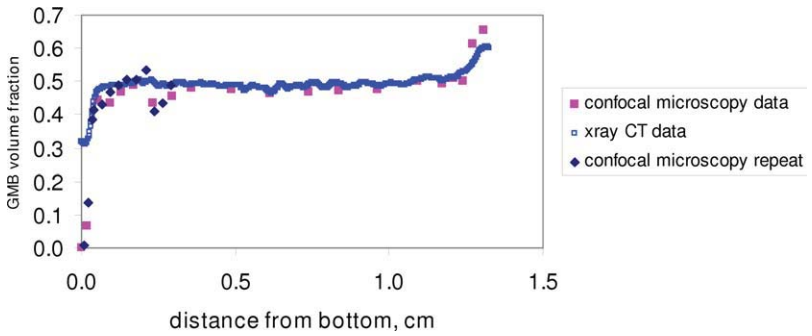

Figure 4 X-ray CT data compared with confocal microscopy data[20] for a plug of 828/DEA filled with GMB. [Color figure can be viewed in the online issue, which is available at wileyonlinelibrary.com.]

pointing out the inherent variations in data taken at this scale. We judge that the advantages of the CT outweighed the disadvantages for the resolution of interest for model validation.

THEORY

Description of suspension model

The suspended particles of interest are noncolloidal and suspended in highly viscous epoxies so the flow is essentially creeping. The constitutive equations used here are based on those used by Rao et al.[8,10] to describe non-neutrally buoyant suspensions under isothermal conditions; however, we replace the constant suspending fluid viscosity by a viscosity that changes with temperature and extent of reaction. For completeness, we summarize the suspension model here.

One of the key features of this model is the density difference between the fluid and the particle phases, which introduces a variable density throughout the flow regime. The total density of the mixture is the sum of mass concentrations of the fluid phase and the particle ("solid") phase:

$$\rho = \rho_f + \rho_s = (1-\phi)\rho_f^0 + \phi\rho_s^0 \tag{1}$$

where ϕ is the particle-phase volume fraction, and ρ_f^0 and ρ_s^0 are the pure phase densities.

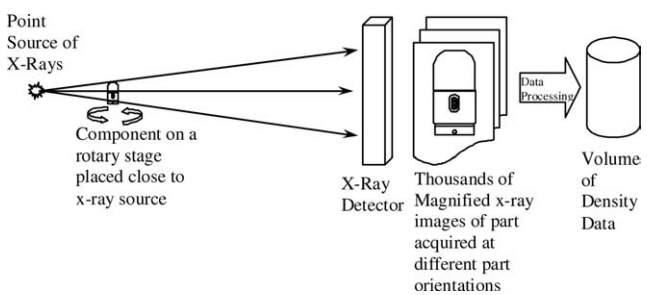

Figure 5 Schematic of x-ray CT technique.

The momentum equation is written:

$$\rho\frac{\partial \mathbf{v}}{\partial t} + \rho\mathbf{v}\cdot\nabla\mathbf{v} + \nabla P - \nabla\cdot\left(\eta\left(\nabla\mathbf{v} + (\nabla\mathbf{v})^T\right)\right) - \left(\rho_f^0 - \rho_s^0\right)\phi\mathbf{g} = 0 \tag{2}$$

where $\mathbf{v}$ is the suspension velocity, P is the dynamic pressure, $\mathbf{g}$ is the gravitational acceleration, and t is time. The viscosity η depends on the particle volume fraction and the time- and temperature-dependent viscosity of the suspending epoxy η_0 (see next subsection). Here, we use a Krieger-like model[24] used by Phillips et al. in the original diffusive flux model development[13]:

$$\eta = \eta_0\left(1 - \frac{\phi}{\phi_m}\right)^{-q} \tag{3}$$

where ϕ_m is the maximum packing fraction. We use the values $q = 1.82$ and $\phi_m = 0.68$ originally proposed by Phillips et al.,[13] which we find also match the viscosity data for GMB in the liquid components fairly well (Fig. 6).

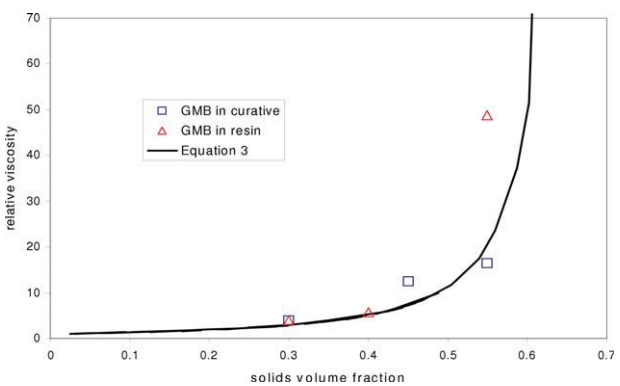

Figure 6 Relative viscosity of suspensions of GMB in either the epoxy resin alone or the curative alone. All measurements reported are taken at a shear rate of 2 s^{-1}. [Color figure can be viewed in the online issue, which is available at wileyonlinelibrary.com.]

As described in Rao et al.,[10] the continuity equation will not be solenoidal because of the density difference between particles and carrier fluid. This introduces the particle flux, $\mathbf{J}_s$, into the continuity equation.

$$\nabla \cdot \mathbf{v} = \frac{\left(\rho_s^0 - \rho_f^0\right)}{\rho_s^0 \rho_f^0} \nabla \cdot \mathbf{J}_s \tag{4}$$

The particle flux is determined from a particle conservation equation,[10] which, when combined with the continuity equation and eq. (1) can be written:

$$\frac{\partial \phi}{\partial t} + \mathbf{v} \cdot \nabla \phi = -\frac{\rho}{\rho_s^0 \rho_f^0} \nabla \cdot \mathbf{J}_s \tag{5}$$

The flux, $\mathbf{J}_s$, is defined as in Phillips et al.[13] and Zhang and Acrivos[14] and describes particle migration from high shear to low shear regions, from high volume fraction to low volume fraction, and due to sedimentation or flotation.

$$\begin{aligned} \frac{\mathbf{J}_s}{\rho_s^0} = &-\left(\phi D_\phi \nabla(\dot{\gamma}\phi) + \phi^2 \dot{\gamma} D_\eta \nabla(\ln \eta)\right) \\ &+ f_{\text{hindered}} \mathbf{v}_{\text{Stokes}} \phi - D_{\text{Fickian}} \nabla \phi \end{aligned} \tag{6}$$

where $\dot{\gamma}$ is the magnitude of the shear-rate tensor

$$\dot{\gamma} = \sqrt{\frac{1}{2}\left(\underset{\sim}{\dot{\gamma}} : \underset{\sim}{\dot{\gamma}}\right)} \quad \text{and} \quad \underset{\sim}{\dot{\gamma}} = \left(\nabla \mathbf{v} + (\nabla \mathbf{v})^T\right) \tag{7}$$

D_ϕ and D_η are parameters that must be fit to data, but which scale as the particle radius (a) squared. Tetlow et al.[25] used experiments and statistical methods to determine a volume fraction dependent D_ϕ, with a constant D_η, and we use a similar relationship.

$$D_\phi = \phi D_\eta \quad D_\eta = 0.62a^2 \tag{8}$$

The buoyancy term is written as a Stokes single particle velocity multiplying a factor less than one termed a "hindered settling function." The Stokes velocity is

$$\mathbf{v}_{\text{Stokes}} = \frac{2}{9} \frac{a^2 \left(\rho_f^0 - \rho_s^0\right) \mathbf{g}}{\eta_0} \tag{9}$$

We use a hindered settling function, f_{hindered}, similar to Zhang and Acrivos,[14] except we use the average volume fraction or a reference volume fraction to determine its value together with the local viscosity. This hindered settling function is found to reduce the occurrence of aphysical shocks that would occur near the zone of maximum packing.[8]

$$f_{\text{hindered}} = \frac{\eta_0 (1 - \phi^{\text{average}})}{\eta} \tag{10}$$

The average volume fraction, ϕ^{average}, is just the initial volume fraction since the problems that we are solving involve closed flows.

To further stabilize the equations near the clear zone, in which problems with oscillations are frequently seen, we use the Fickian diffusivity term shown in eq. (6). This term is purely numerical, used for stabilization only, and there is no Brownian diffusion present. We use a numerical diffusion coefficient that decays away from the clear zone interface. It takes the form:

$$D_{\text{Fickian}} = D_0 e^{-b\phi} \tag{11}$$

Through trial and error, we choose D_0 and b to be as small as possible such that they stabilize the solution but not so large that they interfere significantly with the results. Figure 7 shows a plot of eq. (11) for various values of b. From this, we can see that the Fickian diffusivity is largest near $\phi = 0$ and quickly decays away from there. In this study, we find that numerical stability considerations dictated that we use $D_0 = 1 \times 10^{-3}$ and $b = 10$.

Epoxy reaction kinetics

The apparent viscosity of the liquid epoxy is a strong function of time via the extent of cure, the volume fraction of filler, and temperature.[5,21,26]

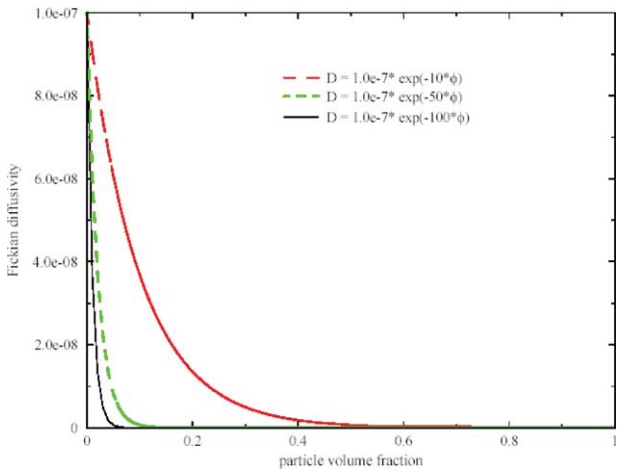

Figure 7 Plot of Fickian diffusivity using the exponential decay function for a variety of parameters b (see equation 11). [Color figure can be viewed in the online issue, which is available at wileyonlinelibrary.com.]

While crosslinking of reacting epoxy is a highly complex process, it generally follows condensation chemistry in which a general kinetics equation can describe the reaction rate R_α in terms of the extent of reaction α.

$$\frac{\partial \alpha}{\partial t} = R_\alpha = (k_1 + k_2 \alpha^m)(1-\alpha)^n \tag{12}$$

$$k_i = A_i e^{\frac{-E_i}{RT}} \tag{13}$$

where k_1 and k_2 are Arrhenius-like rate constants, and m and n are the orders of reaction. For the 459 epoxy, $A_1 = 6.97 \times 10^5$ min^{-1}, $E_1 = 5. \times 10^4$ J/mol, $A_2 = 1.9 \times 10^6$ min^{-1}, $m = 1$, and $n = 1.5$. For details of condensation chemistry and mathematical formula therein, see May.[22]

Epoxy liquid viscosity

The epoxy viscosity depends on temperature, T, filler loading level, ϕ, and extent of reaction, α. To a very good approximation, these effects operate independently, so we can decouple their effects:

$$\eta = \eta_0 f(\phi) g(T) h(\alpha) \tag{14}$$

where η_0 is the proportionality constant, and f, g, and h are arbitrary functions that are defined below.

The dependence on filler loading level is modeled in eq. (3) using the Krieger relationship. The dependence on temperature above the glass transition temperature, T_g, is typically described by the William-Landel-Ferry (WLF) equation.[27] A modification must be incorporated for reacting epoxies due to the increase in T_g with cure (i.e., a changing "reference temperature" in the WLF equation). While many empirical relationships exist for the dependence of T_g on extent of reaction, we previously[4] used the approach of Hale et al.[28] The viscosity temperature dependence can therefore be described by

$$g(T) = 10^{\frac{-C_1(T-T_g)}{C_2+T-T_g}} \quad \text{where} \quad T_g = \frac{T_g^0}{1-A\alpha} \tag{15}$$

and T_g^0, A, C_1, and C_2 are model parameters.

The viscosity increases as the average molecular weight increases during cure. The details of structural evolution in crosslinking epoxies appear to be described well by percolation theory,[29] and Martin et al.[30] related the evolution of epoxy dynamics to this underlying change in structure. The viscosity is predicted to depend on the percolation bond probability, p, in a typical critical phenomena fashion,

$$h(\alpha) = \left(\frac{p_c - p}{p_c}\right)^{-z} \tag{16}$$

where p_c is the critical extent of reaction at the gel point and the critical exponent, z, is ~ 1.33. For condensation reactions, p is proportional to α^2, where α is the extent of reaction; therefore, $p_c \sim \alpha_g^2$, where α_g is the value of α at the gel point.

The composite expression for the evolving shear viscosity, combining eq. (3) with the effects of curing, is given by

$$\eta(\phi, \alpha, T) = \eta\left(0, 0, T_g^0\right)\left(1 - \frac{\phi}{0.68}\right)^{-1.82} \left(1 - \left(\frac{\alpha}{\alpha_g}\right)^2\right)^{-\frac{4}{3}} 10^{-\frac{C_1(T-T_g)}{C_2+T-T_g}} \tag{17}$$

The values of the various constants for our epoxy system are $\eta_0 = 1.5 \times 10^7$ Pa s, $T_g^0 = 260$ K, $\alpha_g = 0.865$, $A = 0.29$, $C_1 = 12.4$, and $C_2 = 43.8$ K. Here, we ignore any normal stresses as they should be small for quiescent settling and for the flow field studied here.[17,18]

Energy balance

Conservation of energy results in a convection–conduction equation for the flow of energy through the domain:

$$\rho C_p \frac{dT}{dt} = -\mathbf{v} \cdot \nabla(\rho C_p T) - \nabla \cdot \mathbf{q} + H(\alpha) \tag{18}$$

where T is the temperature, C_p is the (assumed constant) heat capacity, $\mathbf{q} = -k\nabla T$ is the heat flux by conduction, k is the thermal conductivity, and H is

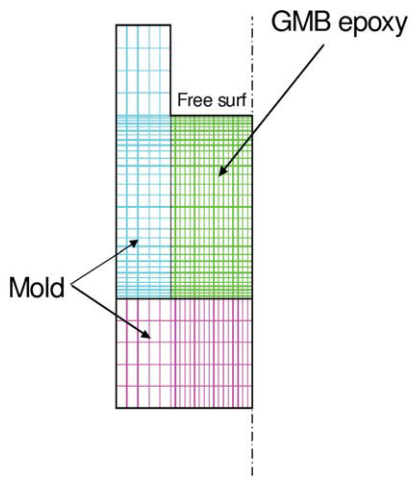

Figure 8 Mesh used to model settling in the geometry shown on the right side of Figure 1. [Color figure can be viewed in the online issue, which is available at wileyonlinelibrary.com.]

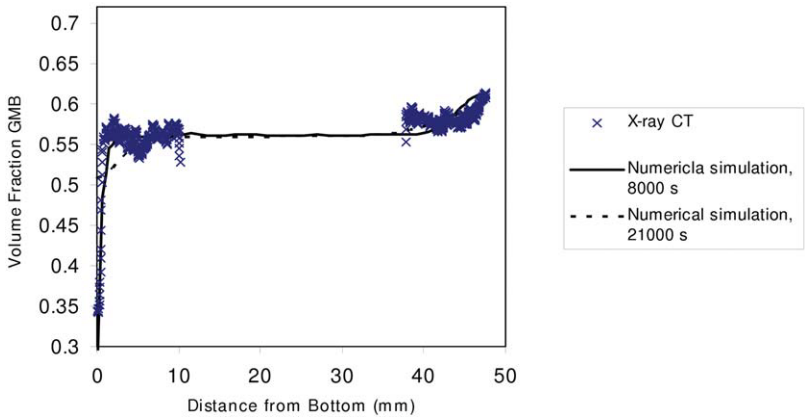

Figure 9 Variations in the volume fraction of GMB particles as a function of height in a simple disk (Fig. 1). Numerical simulation at 8000 s (solid line) are almost indistinguishable from simulations at 21,000 s (dashed line) implying that a steady profile has been reached. The x-ray CT data (×) were only taken at the edges of the domain as shown in Figure 1 and match reasonably well. [Color figure can be viewed in the online issue, which is available at wileyonlinelibrary.com.]

the heat generation due to the curing reaction. H is the product of the heat of reaction, ΔH_{rxn}, and the reaction rate, R_α, defined in eq. (12):

$$H(\alpha) = \Delta H_{rxn} R_\alpha = \Delta H_{rxn} \frac{\partial \alpha}{\partial t} \tag{19}$$

The heat of reaction for our epoxy system is 4.2×10^5 J/kg of epoxy. The epoxy density (without filler) is 1.2×10^3 kg/m^3. C_p for GMB-filled 459 is 1.55×10^3 J/(kg K), based on the mass of the suspension. The thermal conductivity k for GMB-filled 459 is 1.65×10^{-1} J/(s m K). We assume that there is no change in the material's density with changing temperature.

RESULTS

Epoxy systems under quiescent conditions—particle volume fraction

Figure 8 illustrates the mesh corresponding to the geometry on the right side of Figure 1. Figure 9 shows the volume fraction of GMB particles in the 459 curing epoxy, as measured with x-ray CT and as predicted by the model. The computational results show the existence of a front in volume fraction between the clear zone and the suspension immediately above it. This sharp transition is difficult to resolve numerically because the properties here change very rapidly and dramatically. At 8000 s, the computations and the measurements agree well. By 21,000 s (the approximate time of vitrification) the numerical model predicts that the front becomes less sharp, although there is no experimental evidence that this occurs. Since the height of the clear zone ranges from 100 to 200 μm, the resolution of the grid does not allow us to resolve the small height of the clarified region.

The mesh and boundary conditions for the Kovar-tube model (Fig. 2) are depicted in Figure 10. The volume fraction contours predicted by the model are shown in Figure 11. It is apparent that the GMB rises and leaves a region of high particle volume fraction momentarily trapped by the bottom edge of the Kovar tube. Likewise, a zone clear of particles

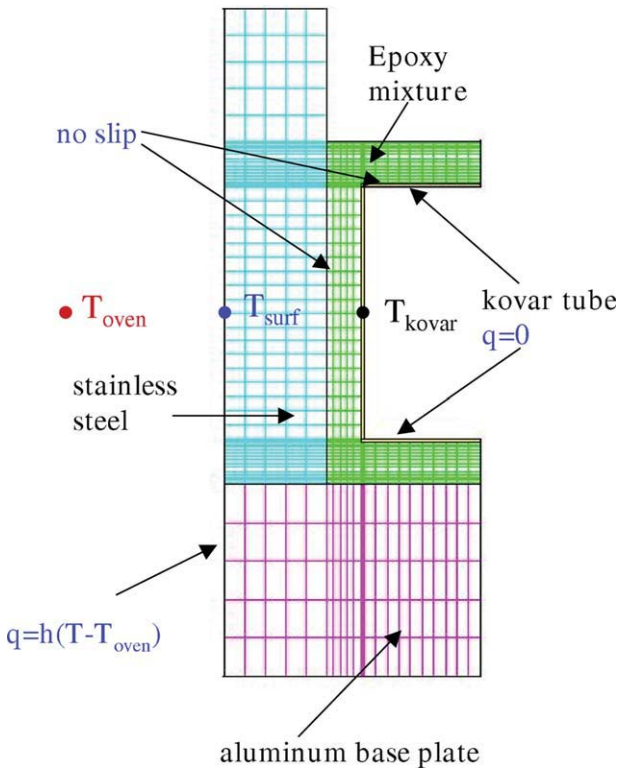

Figure 10 Mesh and boundary conditions for modeling the Kovar tube mold. Right side is an axis of symmetry. [Color figure can be viewed in the online issue, which is available at wileyonlinelibrary.com.]

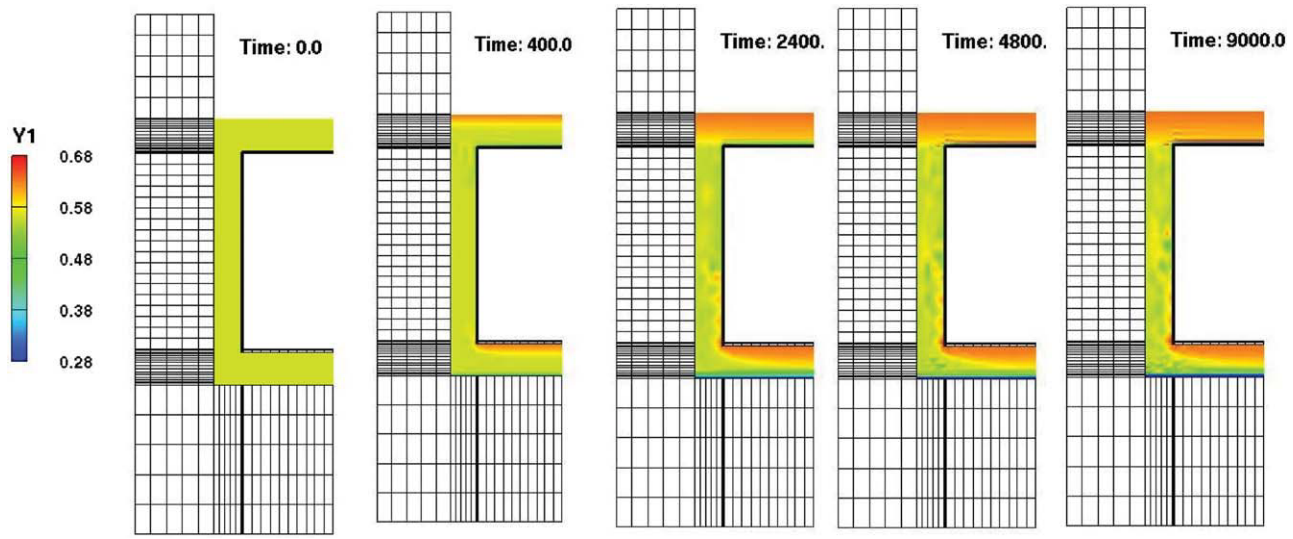

Figure 11 GOMA results show instabilities and complex flow.

momentarily forms at the top edge of the Kovar tube. This creates regions of high density above regions of lower density, a situation which leads to a Raleigh-Taylor instability. From the figure, one can see examples of blobs of heavier epoxy-rich material that sink periodically off the top edge of the Kovar tube and blobs of lighter particle-rich material that spawn from the bottom edge.

Figure 12 shows the results of the CT measurements of GMB volume fraction. In a two-dimensional slice through the axis of the cylinder we examine the volume fraction of GMB along three lines. Directly under the Kovar tube, the volume fraction increases with distance from the bottom from a little over 0.5 to about 0.65 because of particle flotation. These values of volume fraction are in reasonable agreement with the numerical model. Along the outside of the Kovar tube, a crack in the epoxy causes a very low density (which looks like high GMB volume fraction) near the top edge of the Kovar tube. This is labeled as an artifact. Below that is a region of higher density (lower GMB volume fraction) that appears to be an epoxy blob, again in agreement with the model.

Epoxy systems under quiescent conditions—thermal validation

The heat transfer aspects of the calculations are verified by comparing the GOMA calculations with experimental data from the same axisymmetric strain-test mold described above (Fig. 2).[31] The important heat transfer mechanisms included in the simulation are the forced and free convective heat transfer to the mold surface, heat conduction through the various materials of the mold, epoxy suspension and

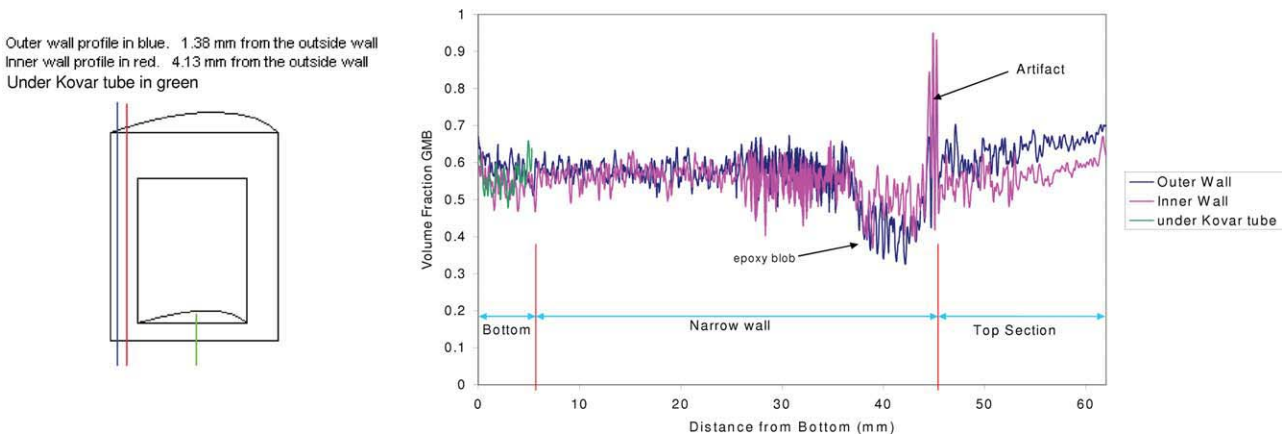

Figure 12 X-ray CT measurements of GMB particle volume fraction (right) along the three lines indicated on the left. [Color figure can be viewed in the online issue, which is available at wileyonlinelibrary.com.]

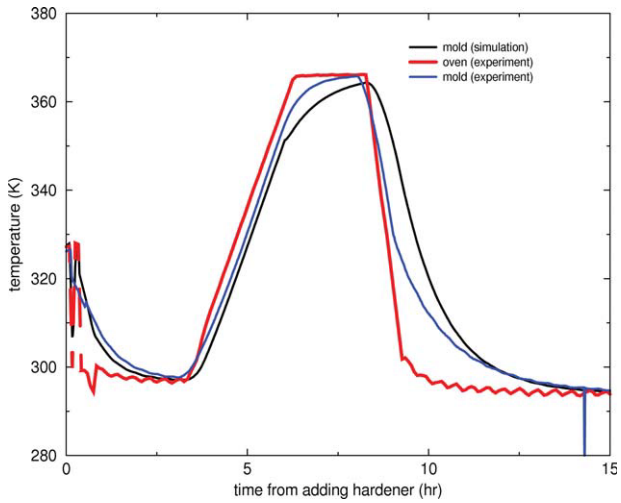

Figure 13 Comparison of measured[31] and computed temperatures on the outside of the stainless steel mold (Fig. 10). [Color figure can be viewed in the online issue, which is available at wileyonlinelibrary.com.]

Kovar tube, as well as heat generation by the cure reaction of the epoxy. Figure 13 shows the predicted and experimental temperatures of the mold outside surface. The red curve shows the measured temperature of the oven as it goes through the programmed temperature profile. For the most part, the agreement between the measured and predicted surface temperatures is reasonable, indicating that the heat transfer coefficient used is also reasonable. The particle tracking calculations do not need to be carried out past 6 h because by this time in the cure, the epoxy is completely solidified and no further particle migration can occur. Later time discrepancies in the

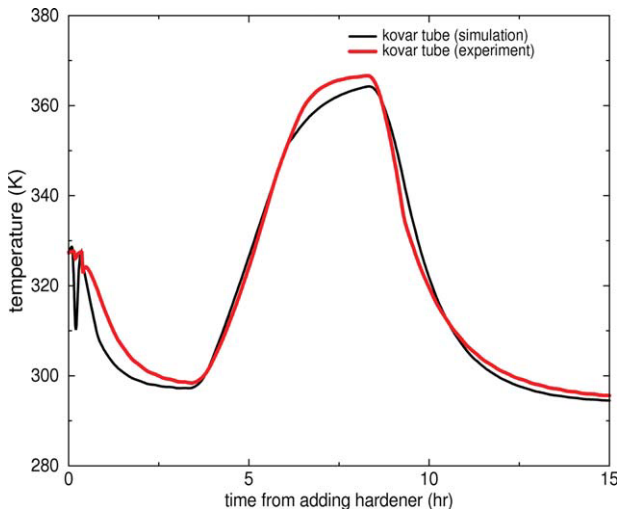

Figure 14 Comparison of measured[31] and computed temperatures at the interface of the GMB/459 epoxy and the Kovar tube. [Color figure can be viewed in the online issue, which is available at wileyonlinelibrary.com.]

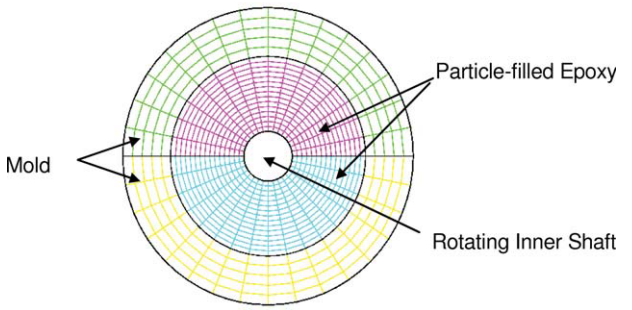

Figure 15 Mesh for Couette geometry. [Color figure can be viewed in the online issue, which is available at wileyonlinelibrary.com.]

predicted and measured temperatures are partly due to the opening of vents in the convection oven part way through the cure. These vents direct the convection oven fan to exhaust outside of the oven, which change the heat transfer mechanism of the surface of the mold from one of forced convection to that of more free convection. Figure 14 shows the predicted temperatures at the surface of the Kovar tube next to the epoxy. Again, agreement between the experiment and the measurements is good, indicating that heat of reaction parameters used in the simulation are reasonable.

Suspension under flow

We also test the suspension under flow conditions by placing the suspension in the wide-gap Couette apparatus described in Figure 3, then rotating the inner rod at 60 rpm as the material cures until vitrification (at about 21,000 s). The mesh corresponding to this geometry is shown in Figure 15.

Computational simulations (Fig. 16) show that the particles not only migrate away from the inner rotating shaft, but also float away from the bottom and toward the top, creating an asymmetrical volume fraction profile at early times. As the flow continues, the suspensions get remixed, and the asymmetries disappear, although the particles migrate away from the higher shear-rate regions near the rotating inner shaft to form a radial volume fraction gradient. Figure 17 shows x-ray CT data after cure, both the raw data and a trendline showing a running average of five data points, along a line across the diameter of the Couette apparatus taken from the bottom to the top near the middle of the apparatus length. Plotted also are the numerical predictions at the time when the rotation is stopped. Edge effects are no doubt present because of the high contrast between the aluminum shaft and the epoxy. This makes the density near the shaft appear too high and, hence, the

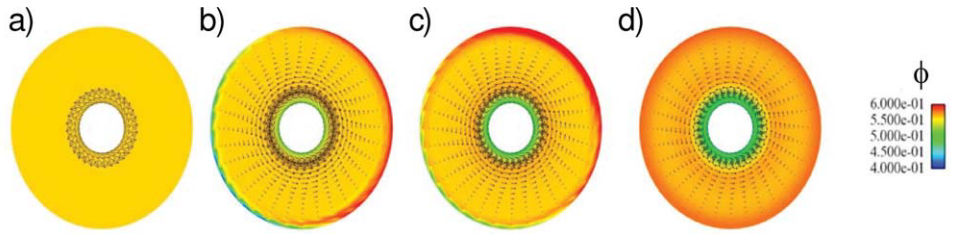

Figure 16 Velocity vectors and volume fraction as a function of time: a) $t = 0$ s, b) $t = 102$ s, c) $t = 404$ s, d) $t = 24140$ s.

volume fraction of the light particles appear too low. Nonetheless, the model predictions underestimate the particle migration away from the shaft somewhat. Figure 18 shows the comparison for two thermocouple locations, at the inner wall of the Couette apparatus and within the epoxy about 2.5 cm from one end. Again, simulation and measurements agree well.

DISCUSSION

We present work in modeling coupled thermal effects and suspension rheology of filled curing epoxies and in validating the resulting model. Two mold geometries are studied in which the bulk suspension is quiescent, although gravity effects drive convective flow. Flow of a suspension in a wide-gap Couette apparatus is also studied to provide a case in which flow-induced migration might occur to a larger extent given the imposed flow field.

The GMB particles float to a measurable extent in our experiments in the simplest molds. The model in general predicts the flotation reasonably well; however, numerical instabilities tend to occur in the region of sharp particle volume fraction change near the clarification zone. Across this clarification zone, the viscosity can increase exponentially as the volume fraction of suspended particles increases. These numerical difficulties lead to the need for the addition of a Fickian diffusivity term which can in turn lead to nonphysical smoothing of the predicted profiles at long times.

For sedimentation in more complex geometries, the modeling indicates that density-driven (Rayleigh-Taylor) instabilities can lead to complex flow patterns. These flow patterns actually cause remixing of the suspension and can reduce the numerical difficulties in the modeling. This has also been seen in noncuring examples described by Rao et al.[8] Post test analyses of cured samples are consistent with this conclusion, as shown by a concentrated "blob" of material present in Figure 12.

Suspended particles not only settle due to gravity but can migrate across streamlines when subjected to gradients in shear rate. Although the model captures qualitatively the effects of shear-induced migration, the model underpredicts the amount of

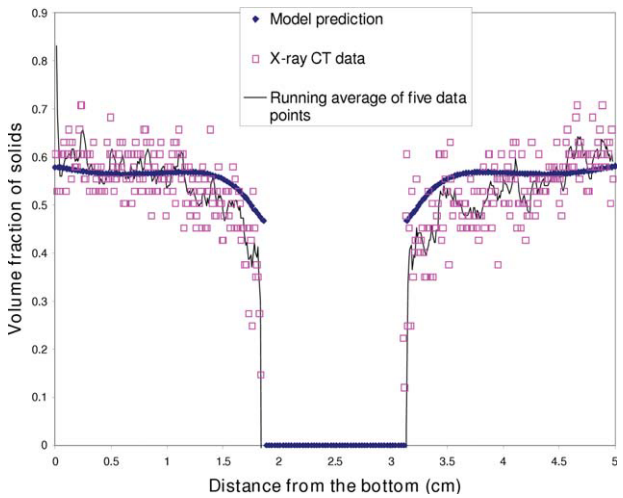

Figure 17 Comparison of GOMA calculation and x-ray CT data along two lines from the inner shaft to the outer wall. [Color figure can be viewed in the online issue, which is available at wileyonlinelibrary.com.]

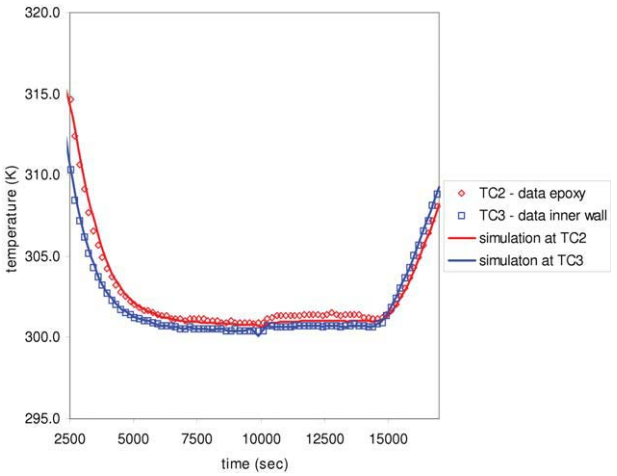

Figure 18 Comparison of simulation and measured temperatures in a Couette during shaft rotation. [Color figure can be viewed in the online issue, which is available at wileyonlinelibrary.com.]

particle movement. This shortfall of the model is most likely to be caused by the particle migration formulation rather than the model of the coupling of viscosity to cure kinetics, because the diffusive flux model, as well as other models in which the migration rate depends on the particle radius squared, have been shown to underpredict the migration rate in many situations.[18,25,32] Nevertheless, the modeling can correctly show trends that occur in the particle volume fraction.

Coupling of the viscosity to the cure kinetics and accounting for the heat of reaction is also shown to be possible in these models. Accurate prediction of the temperature history of the epoxy suspension is vital for meaningful prediction of particle volume fraction changes during the cure process for a number of reasons. The epoxy temperature affects the suspension viscosity in two important ways. First, the epoxy viscosity is directly related to temperature: the higher the temperature, the lower the viscosity. Second, the epoxy viscosity is also related to the degree of cure, which is accelerated by temperature: the higher the temperature, the faster the cure and thus the higher the epoxy viscosity. The epoxy suspension viscosity is also a strong function of the particle volume fraction: the higher the particle loading, the higher the suspension viscosity. The net result is an exponential increase in viscosity with time that can span three orders of magnitude. Initially, the material is less viscous from thermal effects. At later times, the epoxy cure and particle effects dominate the viscosity. The close tie of epoxy temperature to viscosity, which greatly influences the particle movement in the suspension, points to the importance of validation of the thermal and heat transfer aspects of the computational simulation.

In conclusion, this work underscores the usefulness of both x-ray CT and computational modeling for understanding the complex behavior of suspensions of non-neutrally buoyant particles in flowing, polymerizing systems. The validated model can help us design better manufacturing processes involving suspensions in reasonably complex geometries.

Sandia is a multiprogram laboratory operated by Sandia Corp., a Lockheed Martin Company, for the United States Department of Energy.
The authors would also like to thank Becky Lee, University of New Mexico, for help with the confocal microscopy, and Mark Stavig, Sandia National Laboratories, for help in obtaining data in the Kovar tube geometry.

References

1. Anderson, R. A.; Lagasse, R. R.; Russick, E. M.; Schroeder, J. L. J Appl Phys 2002, 91, 3205.
2. Varley, R. J. Macromol Mater Eng 2007, 292, 46.
3. Hashmi, S. A. R. J Appl Polym Sci 2006, 99, 3009.
4. Adolf, D.; Martin, J. E. J Compos Mater 1996, 30, 13.
5. Adolf, D.; Strommen, R.; Johnson, H. Viscosity of Epoxy Encapsulants, Sandia National Laboratories, SAND97-2631 1997.
6. Metzner, A. J Rheol 1985, 29, 739.
7. Love, B. J. Particulate Sci Technol 2004, 22, 285.
8. Rao, R. R.; Mondy, L. A.; Altobelli, S. A. Int J Numerical Methods Fluids 2007, 55, 723.
9. Leighton, D.; Acrivos, A. Chem Eng Sci 1986, 6, 1377.
10. Rao, R. R.; Mondy, L. A.; Sun, A.; Altobelli, S. A. Int J Numerical Methods Fluids 2002, 39, 465.
11. Gao, J. W.; Wang, C. Y. Mater Sci Eng 2000, A292, 207.
12. Hashmi, S. A. R.; Dwivedi, U. K. Polym Eng Sci 2006, 46, 1660.
13. Phillips, R. J.; Armstrong, R. C.; Brown, R. A.; Graham, A. L.; Abott, J. R. Phys Fluids A 1992, 4, 30.
14. Zhang, K.; Acrivos, A. Int J Multiphase Flow 1994, 20, 579.
15. Nott, P. R.; Brady, J. F. J Fluid Mechanics 1994, 275, 157.
16. Buyevich, Y. U. A. Chem Eng Sci 1995, 50, 641.
17. Morris, J. F.; Boulay, F. J Rheol 1999, 43, 1213.
18. Fang, Z.; Mammoli, A. A.; Brady, J. F.; Ingber, M. S.; Mondy, L. A.; Graham, A. L. Int J Multiphase Flow 2002, 28, 137.
19. Schunk, P. R.; Sackinger, P. A.; Rao, R. R.; Chen, K. S.; Baer, T. A.; Labreche, D. A.; Sun, A. C.; Hopkins, M. M.; Subia, S. R.; Moffat, H. K.; Secor, R. B.; Roach, R. A.; Wilkes, E. D.; Noble, D. R.; Hopkins, P. L.; Notz, P. K.; GOMA 5.0 - A Full-Newton Finite Element Program for Free and Moving Boundary Problems with Coupled Fluid/Solid Momentum, Energy, Mass, and Chemical Species Transport: User's Guide, Sandia National Laboratories, SAND2006-5375/1, October 2006.
20. Lagasse, R. R.; Thompson, K. Polymer 2002, 43, 803.
21. Adolf, D. Measurement Techniques for Evaluating Encapsulant Thermophysical Properties During Cure, Sandia National Laboratories, SAND96-1458 1996.
22. May, C. A., Ed. Epoxy Resins Chemistry and Technology, 2nd ed.; Marcel Dekker: New York, 1988.
23. Lee, B. University of New Mexico, personal communication, July 2002.
24. Krieger, I. M. Adv in Colloid Interface Science 1972, 3, 111.
25. Tetlow, N.; Graham, A. L.; Ingber, M. S.; Subia, S. R.; Mondy, L. A.; Altobelli, S. A. J Rheol 1998, 42, 307.
26. Castro, J. M.; Macosko, C. W. Am Inst Chem Eng J 1982, 28, 250.
27. William, M. L.; Landel, R. F.; Ferry, J. D. J Am Chem Soc 1955, 77, 3701.
28. Hale, A.; Macosko, C. W.; Bair, H. E. Macromolecules 1991, 24, 2610.
29. Adolf, D. B.; Martin, J. E.; Wilcoxon, J. P. Macromolecules 1990, 23, 527.
30. Martin, J. E.; Adolf, D. B.; Wilcoxon, J. P. Phys Rev A 1989, 39, 1325.
31. Guess, T. R.; Stavig, M. E. Curing Strains in Epoxy Encapsulants: Experimental Data for Model Validation Studies, Sandia National Laboratories, SAND2000-2206 2000.
32. Ingber, M. S.; Graham, A. L.; Mondy, L. A.; Fang, Z. Int J Multiphase Flow 2009, 35, 270.